

c-di-GMP modulates ribosome assembly by inhibiting rRNA methylation

Siqi Yu^{1,2,3#}, Zheyao Hu^{4#}, Xiaoting Xu^{1,3,5#}, Xiaoran Liang^{1,2,3}, Jiayi Shen^{1,2,3},
Min Liu^{1,2,3}, Mingxi Lin^{1,2,3}, Hong Chen⁶, Jordi Marti^{4*}, Sheng-ce Tao^{6*},
Zhaowei Xu^{1,2,3*}

¹Key Laboratory of Gastrointestinal Cancer (Fujian Medical University),
Ministry of Education, Fuzhou, China

²Laboratory of Scientific Research, School of Basic Medical Sciences, Fujian
Medical University, Fuzhou, China

³Fujian Key Laboratory of Tumor Microbiology, Department of Medical
Microbiology, Fujian Medical University, Fuzhou, China

⁴Department of Physics, Polytechnic University of Catalonia-Barcelona Tech,
Barcelona, Catalonia, Spain

⁵Department of Endoscopy, The First Affiliated Hospital of Fujian Medical
University, Fuzhou, China

⁶Shanghai Center for Systems Biomedicine, Key Laboratory of Systems
Biomedicine (Ministry of Education), Shanghai Jiao Tong University, Shanghai,
China

[#]These authors contributed equally to this study.

^{*}Corresponding authors. E-mail: xuzw@fjmu.edu.cn (Zhaowei Xu),
taosc@sjtu.edu.cn (Sheng-ce Tao), jordi.marti@upc.edu (Jordi Marti)

Highlights

1. c-di-GMP regulates ribosome assembly in *Escherichia coli*.
2. c-di-GMP inhibits rRNA methylation activity of RlmI by inducing catalytic pocket closure.
3. c-di-GMP promotes antibiotic resistance by regulating ribosome assembly.

Abstract

Cyclic diguanosine monophosphate (c-di-GMP) is a ubiquitous bacterial secondary messenger, with diverse functions, many of which are yet to be uncovered. Stemming from an *Escherichia coli* proteome microarray, we found that c-di-GMP bound to 23S rRNA methyltransferases (RlmI and RlmE). rRNA methylation assays showed that c-di-GMP inhibits RlmI activity, thereby modulating ribosome assembly. Based on molecular dynamic simulation and mutagenesis studies, we found that c-di-GMP binds to RlmI at residues R64, R103, G114, and K201. Structural simulation revealed that c-di-GMP quenches RlmI activity by inducing the closure of the catalytic pocket. Furthermore, we revealed that c-di-GMP promotes antibiotic tolerance by regulating RlmI activity, which played a role in antibiotic-resistant strains. Finally, the binding and methylation assays showed that the effect of c-di-GMP on RlmI is conserved, at least in various pathogenic bacteria. This study discovered an unexpected functional role of c-di-GMP in regulating ribosome assembly by inhibiting rRNA methylases. This study identified an unexpected but crucial member among the c-di-GMP effectors.

Keywords: c-di-GMP; rRNA methyltransferase; ribosome assembly; antibiotic tolerance

Introduction

Cyclic diguanosine monophosphate (c-di-GMP) was first identified in *Gluconacetobacter xylinus*, where it regulated cellulose synthesis¹. Subsequent research revealed that c-di-GMP plays a role in a wide range of bacterial biological processes, such as motility, virulence, and host-microbe symbiosis²⁻⁵. In a previous study, we globally screened c-di-GMP binding proteins by applying an *Escherichia coli* proteome microarray and revealed the interplay loop between c-di-GMP and protein acetylation⁶. Interestingly, the microarray assay also showed that 23S rRNA methyltransferases RlmI and RlmE act as c-di-GMP binding proteins. This suggests a functional link between c-di-GMP and ribosome assembly.

The ribosome assembly involves the processing and folding of rRNA and its concomitant assembly with ribosomal proteins. As a part of rRNA processing, rRNA methylation participates in the regulation of ribosome assembly. For example, the inactivation of RlmE is associated with a large subunit assembly defect⁷, and RsmA fulfills quality control requirements in the last stages of small subunit assembly⁸. Overall, 23 ribosomal RNA methylases exist in *E. coli*, most of which have unresolved physiological functions. Consequently, studying the function and regulatory factors of rRNA methyltransferase is crucial for understanding the mechanism of ribosome assembly.

Ribosome biogenesis is a fundamental cellular process, equipping cells with the molecular factories for cellular protein production. Inhibiting ribosome assembly is considered an essential source of new targets for drug development^{9,10}. Therefore, studying the relationship between ribosome assembly and bacterial resistance is crucial for designing antibiotics targeting ribosome assembly pathways. In Gram-positive bacteria, (p)ppGpp negatively impacts ribosome assembly by inhibiting GTPase activity, influencing growth and antibiotic tolerance¹¹. However, in Gram-negative bacteria, the influence of (p)ppGpp on antibiotic tolerance mainly affects nucleotide and amino acid synthesis^{12,13}. The regulatory relationship between ribosome assembly and antibiotic tolerance in Gram-negative bacteria is yet to be understood.

rRNA methylation serves as a significant mechanism for bacterial resistance against ribosome-targeting antibiotics. Two clinically relevant examples include 16S and 23S rRNA methyltransferases, which confer resistance by modifying conserved rRNA residues in site A or PTC, respectively. This modification makes bacteria insensitive to aminoglycosides and streptogramin B¹⁴. For instance, aminoglycoside resistance in *E. coli* is conferred by methylation of the G1405 and A1408 residues in the 16S rRNA by RsmF¹⁵ and NpmA¹⁶, respectively. The Erm macrolide-resistance methyltransferase family has been widely identified in Gram-positive bacteria¹⁷ and continued to spread and mutate

globally^{18,19}. The chloramphenicol-florfenicol resistance (*cfr*) SAM methyltransferase family shares ancestry with the housekeeping RlmN methyltransferases. These methyltransferases incorporate methylation at A2503 in 23S rRNA and A37 in tRNAs^{20,21}. However, the upstream regulatory factors and downstream mechanisms of rRNA methylation in the context of antibiotic resistance remain unclear.

In this study, we demonstrate that c-di-GMP binds to four 23S rRNA methyltransferases and that RlmI is the main effector of c-di-GMP in regulating ribosome assembly. Structural analysis revealed that c-di-GMP binds to RlmI at the R64, R103, G114, and K201 residues and induces the closure of the catalytic pocket of RlmI. We further show that c-di-GMP regulates ribosomal assembly to promote antibiotic resistance by inhibiting RlmI activity. Finally, sequence comparison of RlmI orthologues among bacteria indicated that some important human pathogens are conserved in the c-di-GMP-based rRNA regulation mechanism.

Material & Methods

E. coli strains and plasmids

E. coli BW25113 as reference strain was used in this study, and pCA24N and pGEX4T-1 plasmids were used to overexpress methyltransferases and their mutants. Further, pET28a was used for RlmI of *S. typhimurium*,

K. pneumoniae, and *V. cholerae*. We performed recombinant RlmI mutations using a QuikChange Site-Directed Mutagenesis Kit (#200518, Agilent Technologies, USA).

The strains described earlier were grown in Vogel-Bonner medium (0.81 mM MgSO₄·7H₂O, 43.8 mM K₂HPO₄, 10 mM C₆H₈O₇·H₂O, and 16.7 mM NaNH₄HPO₄·4H₂O) with 10 mM acetate at 25°C for functional analysis. For kanamycin treatment, 3 µg/mL kanamycin was added to the Vogel-Bonner medium.

For protein purification, the strains were grown in Lysogeny broth (10 g tryptone, 5 g yeast extract, 10 g NaCl per 1 L) medium (LB medium), and then induced by 0.2 mM IPTG at 22°C for 12 h.

Construction of endogenous DgcZ and RlmI mutants in E. coli

DgcZ and RlmI mutants were constructed using the Red-recombination system based on *E. coli* BW25113 strain²², as discussed previously²³. For kanamycin-resistant *E. coli* strains, the *rlmI*^{K201A} mutants were constructed using the Red-recombination system with ampicillin as the screening antibiotic.

Methyltransferase activity assay in vitro

For *in vitro* methylation assays, 3 µM recombinant enzymes (RlmI and RlmE) and c-di-GMP (at either 5 µM, 10 µM, or 20 µM) were incubated

in 20 μ L reaction buffer (40 mM HEPES, 100 mM NH_4Cl , 10 mM MgCl_2 , 1 mM AdoMet, pH 7.6) at 37°C for 0.5 h. Then, 5 μ M rRNA substrates were added and incubated at 37°C for 1.5 h. Reactions were stopped by heating at 95°C for 10 min and centrifugation at 10,000 x g for 10 min at 4°C to remove sediments.

These samples were analyzed by HPLC. Briefly, the samples were injected into a C-18 column (Alltima C18 4.6 250 mm²) and analyzed by reversed-phase HPLC (Shimadzu, Japan). Solution A [0.065% trifluoroacetic acid in 100% water (v/v)] and solution B [0.05% trifluoroacetic acid in 100% acetonitrile (v/v)] were used in a gradient program (0.01 min with 5% Solution B, 20 min with 65% Solution B, 20.01 min with 95% Solution B, 31 min with 95% Solution B, 31.01 min with 5% Solution B, 40 min with 5% Solution B, and stop in 40.01 min) with a flow rate of 1 mL/min. rRNA was detected at 220 nm, and the area under the curve was integrated for the relative quantification of reaction products. This assay was performed in triplicate, and the results were calculated using GraphPad Prism 6.

MeRIP-qPCR quantification of the endogenous C1962 methylation of 23S rRNA

E. coli strains, such as WT, ΔdgcZ , $\text{rlmI}^{\text{K201A}}$ and $\Delta\text{dgcZ rlmI}^{\text{K201A}}$ were cultivated in LB medium at 37°C overnight and transferred to

163 Vogel-Bonner medium at a 1:1000 ratio with 10 mM acetate and 3 µg/mL
164 kanamycin for 25°C for 24 h. Twenty OD cells were harvested for RNA
165 extraction using an RNA extraction kit (Sangon Biotech, China). Total
166 RNA (50 µg) was diluted in 200 µL of IP buffer (20 mM HEPES, 50 mM
167 KCl, 1 U/µL protector RNase inhibitor, pH=7.5) and treated with a
168 sonicator (Sonics and Materials, USA) (20 cycles on 35% power, 15 s
169 on/off) to prepare the RNA fragments, which were divided into 50 µL as
170 input and 150 µL for IP. Then, 2 µL of anti-m5C antibody was added to
171 150 µL of RNA fragments and incubated at 4°C for 4 h. 20 µL Protein
172 A/G beads (Thermo Fisher Scientific, USA) were added to the mixture
173 and incubated at 4°C for 1 h. The RNA was eluted with 0.1 M glycine
174 (pH = 2) and neutralized with 1.0 M Tris (pH = 8). The eluted RNA and
175 RNA fragments were purified by phenol–chloroform and quantified using
176 a NanoDrop 2000 spectrophotometer (Thermo Fisher Scientific).
177 Real-time RT-PCR was performed using a reverse transcription kit and
178 real-time PCR kit (Applied Biosystems, USA). The following primers
179 were used.

180

	Sequence1 (5'→3')	Sequence2 (5'→3')
C1962	CGGTCCTAAGGTAGCGAAAT	ACGGCGGCCGTA ACTATA
	ACTGAGTCTCGGGTGGAGA	GCCTGGCCATCATTACGCC
23S rRNA	AGTGGAAGCGTCTGGAAAGG	ATCGTACCCCAAACCGACAC
	GCCCTACTCATCGAGCTCAC	TTCTCCCGAAGTTACGGCAC

181

182 *Isolation and antimicrobial susceptibility test of E. coli*

183 The soil samples were dissolved in phosphate-buffered saline, and large
184 particles were removed using static precipitation. The supernatant was
185 plated into MacConkey agar, followed by incubation at 37°C for 18 h.
186 The pink, round, medium-sized colonies were picked as *E. coli* colonies.
187 The antimicrobial susceptibility of the *E. coli* strains was determined by
188 the Kirby-Bauer assay. Briefly, *E. coli* was inoculated into
189 Mueller-Hinton agar (Sigma Aldrich, USA), and 30 µg kanamycin K
190 (Liofilchem, Italy) was used for the antimicrobial susceptibility test.
191 When the zone diameter was less than 13 mm, *E. coli* was considered
192 resistant to kanamycin. The IMViC test kit (HiMedia, India) was
193 employed to confirm the *E. coli* strains.

194 Urine samples were obtained from 8 healthy volunteers. 20 mL urine
195 was centrifuged by 8000 g for 10 minutes and the precipitate was
196 resuspended in 1 mL PBS. The method of isolation and antimicrobial
197 susceptibility test consistent with the above. The study was approved by
198 the Ethical Committee of Fujian Medical University, Fuzhou, China
199 (2022-120).

200 The minimal inhibit concentrations (MICs) of WT and RlmI^{K201A}
201 mutants were determined by ETEST (kanamycin 0.016-256 µg/mL;
202 Liofilchem).

203

204 ***Measuring the relative mRNA levels of methyltransferase***

205 *E. coli* strains such as WT, *dgcZ*⁺ and *dgcZ*^{G206A,G207A} were cultivated in
206 LB medium at 37°C overnight and transferred to Vogel-Bonner medium
207 at a 1:1000 ratio with 10 mM acetate at 25°C for 12 h and then induced
208 with 0.2 mM IPTG at 25°C for 20 h. Ten OD cells were harvested for
209 RNA extraction using an RNA extraction kit (Sangon Biotech, China).
210 Real-time RT-PCR was performed using a reverse transcription kit and
211 real-time PCR kit (Applied Biosystems, USA) with three replicates. The
212 following primers were used.

	Sequence1 (5'→3')	Sequence2 (5'→3')
<i>rlmI</i>	GAAGCGCTGGATATTGCACG	ACGTTTGACCCGTCTGAGTC
	ATCGCGATAAGTACGCAGCA	GTCGAGGCCATCTTTTTCGCG
<i>rlmE</i>	TGGCGCTAGAAATGTGTCGT	GGCGCTAGAAATGTGTCGTG
	ACCTTCGTAAACAGGGAGCG	CCTTCGTAAACAGGGAGCGA
<i>gapA</i>	GATGGCCCGTCTCACAAAGA	TTGACCTGACCGTTCGTCTG
	TGCCATTCAAGTTCTGGCAGT	ACGTCATCTTCGGTGTAGCC

213

214 ***Analysis of ribosomal subunits by sucrose density gradient***

215 ***centrifugation***

216 *E. coli* strains were cultivated in LB medium at 37 °C overnight and
217 transferred to Vogel-Bonner medium at a 1:1000 ratio with 10 mM
218 acetate and 3 µg/mL kanamycin for 25°C for 24 h. Twenty OD cells were
219 harvested and repeatedly freeze–thawed three times. The cells were

treated with 1 mL of lysis buffer (20 mM HEPES, 0.5 mM MgCl₂, 200 mM NH₄Cl, 1 mg/mL lysozyme, 50 units/mL benzonase, pH 7.5) at 4°C for 20 min with vigorous shaking. After lysis and centrifugation at 10,000 × *g* for 10 min at 4°C. The supernatant lysate was layered on top of a sucrose gradient (10%-50%, w/v) in lysis buffer and separated by ultracentrifugation in a Beckman SW-28 Rotor at 120,000 × *g* for 12 h at 4°C. The suspension was recovered to 25 components and quantified by measuring the absorbance at 260 nm on a NanoDrop 2000 spectrophotometer.

Molecular dynamics simulations

The computational tool has been microsecond-scale molecular dynamics (MD) simulation²⁴. In MD simulation, the corresponding Newton's equations of motion are integrated numerically after choosing reliable force fields, allowing us to monitor each individual atom in the system in a wide variety of setups, including liquids at interfaces, in solid walls or biological membranes, among others^{25,26}. The number of particles and the pressure and temperature of the system were fixed, whereas the volume was adjusted accordingly. MD simulation can model hydrogens at the classical or quantum levels²⁷. Besides its energetic and structural properties, it provides access to time-dependent quantities such as diffusion coefficients or spectral densities, enhancing its applicability. In

the present study, we conducted MD simulations of c-di-GMP bound at rRNA methyltransferases (RlmI). The simulation system contained one rRNA methyltransferase and 7 c-di-GMP molecules fully solvated by 21,818 TIP3P water molecules in potassium chloride solution at the 0.15 M concentration, yielding a system size of 68,532 atoms. In each of the two statistically independent MD simulations, one single c-di-GMP molecule was placed at the center of the simulation box, near domains I, II and III of RlmI, whereas the remaining 6 free c-di-GMPs were randomly distributed around the RlmI protein according to the default settings of Charmm-GUI “Multicomponent Assembler”. All MD simulation inputs were generated using the CHARMM-GUI platform^{28,29}, and the CHARMM36m force field³⁰ was adopted for interactions between rRNA methyltransferases and c-di-GMP. The force field used also included the parameterization of the species c-di-GMP. All bonds involving hydrogens were set to fixed lengths, allowing fluctuations of bond distances and angles for the remaining atoms. The crystal structure of rRNA methyltransferases was downloaded from RCSB PDB Protein Data Bank (file name “3c0k”). The system was energy-minimized for 50,000 steps and well-equilibrated (NVT equilibration in Figure 16 of SI) for 250 ps before the production of MD simulation. Production runs were performed with an NPT ensemble for 2 μ s. The pressure and temperature were set at 1 atm and 310.15 K, respectively, to simulate the human body

environment. The GROMACS 2021 package was employed in all MD simulations³¹. Time steps of 2 fs were used in production simulations, and the particle mesh Ewald method with a Coulomb radius of 1.2 nm was employed to compute long-range electrostatic interactions. The cutoff for Lennard–Jones interactions was set to 1.2 nm. The pressure was controlled with a Parrinello-Rahman piston with a damping coefficient of 5 ps⁻¹, whereas the temperature was controlled using a Nosé-Hoover thermostat with a damping coefficient of 1 ps⁻¹. Periodic boundary conditions in three directions of space were considered. We employed the “gmx-sham” tool of the GROMACS 2021 package to perform the Gibbs free energy landscape analysis. Moreover, the software VMD³² and UCSF Chimera³³ were used for trajectory analysis and visualization.

The radius of gyration R_g , used as a reaction coordinate in the computation of Gibbs free energy landscapes, was determined as follows:

$$R_g = \sqrt{\frac{\sum_i ||r_i||^2 m_i}{\sum_i m_i}} \quad (1)$$

where m_i is the mass of atom i , and r_i is the position of the same atom with respect to the center of mass of the selected group. RMSD was calculated as follows:

$$RMSD(t) \equiv \sqrt{\frac{1}{N} \sum_{i=1}^N \delta_i^2(t)} \quad (2)$$

where δ_i is the difference in distance between atom i [located at $x_i(t)$] of the catalytic domain and the equivalent location in the crystal structure.

285 RMSF values were obtained as follows:

$$RMSFi \equiv \sqrt{\sum_{t_j=1}^{\Delta t} (x_i(t_j) - \tilde{x}_i)^2},$$

286 where \tilde{x}_i is the time average of x_i , and Δt is the time interval at which
287 the average was taken.

288

289 *ITC assay*

290 In the ITC assay, c-di-GMP (#C057 of Biolog), RlmI, and its mutants
291 were prepared in titration buffer (20 mM Tris, 50 mM NaCl, 200 mM
292 KCl, pH 7.0). Protein concentrations were measured based on Coomassie
293 brilliant blue staining. The ITC titrations were performed using a
294 MicroCal iTC200 system (GE Healthcare, PA, USA) at 25°C. Each
295 titration process involved 22 injections with 5 µL c-di-GMP. The stock
296 solution of c-di-GMP at 0.5 mM was titrated into WT or mutant RlmI (25
297 µM) in sample cells of 200 µL volume individually. c-di-GMP was
298 titrated into 200 µL titration buffer as a control for subsequent data
299 processing. The resulting titration curves were processed using the Origin
300 7.0 software program (OriginLab) according to the “one set of sites”
301 fitting model.

302

303 *Streptavidin blotting assay*

304 In this assay, RlmI (0.1 mg/mL) and its mutants were incubated with 10

μM biotin-c-di-GMP in a reaction buffer (20 mM Tris, 50 mM NaCl, 200 mM KCl, pH 7.0) at 37°C for 1 h. These samples underwent UV-crosslinking on ice for 0.5 h to further link c-di-GMP to RlmI. These linked samples were divided into two parts for analysis by western blotting. After incubation with IRDye 800CW Conjugated Streptavidin (#926-32230; LI-COR Biosciences, USA) at room temperature for 2 h, another membrane was incubated with anti-His antibody (05-949, Millipore, USA) at 4°C for 12 h and then incubated with an IRDye 800 secondary antibody for 1 h. The resulting membranes were visualized with an Odyssey Infrared Imaging System (LI-COR Biosciences).

Isolation and quantification of c-di-GMP in E. coli

The c-di-GMP isolation was performed as discussed previously^{6,34}. Briefly, *E. coli* cells with 50 OD were harvested and resuspended in 2 mL of ddH₂O. Further, 8 mL of the mixture containing 50% methanol and 50% acetonitrile was added to extract intracellular c-di-GMP. Meanwhile, 1 μM cGMP was added as the internal reference. For c-di-GMP absolute quantification, the density of *E. coli* sediment is defined as 1 mg/mL. The extracts were analyzed by ultra-high-performance liquid chromatography coupled with ion mobility mass spectrometry (UPLC-IM-MS). UPLC-IM-MS was performed using a Waters UPLC I-class system equipped with a binary solvent delivery manager and a sample manager

coupled with a Waters VION IMS Q-TOF mass spectrometer equipped with an electrospray interface (Waters Corporation, CT, USA).

Determination of the strain growth curve in Vogel-Bonner medium

As discussed above, the strains WT, $\Delta dgcZ$, $rlmI^{K201A}$ and $\Delta dgcZ$ $rlmI^{K201A}$ were grown in Vogel-Bonner medium with 10 mM acetate at 25°C. For kanamycin treatment, 0, 1.5, 3, 6 and 9 µg/mL kanamycin was added to the Vogel-Bonner medium, respectively. These cell concentrations were measured at OD₆₀₀ using NanoDrop 2000 spectrophotometer at 8, 12, 16, 24, and 32 h. Then, the growth curve was drawn using GraphPad Prism 6.

Statistical analysis

Pairwise comparisons were performed using two-tailed Student's *t*-test, and statistical significance was set at **p* < 0.05, ***p* < 0.01. Error bars represent the mean ± range.

Results

Ribosomal RNA large subunit methyltransferases are c-di-GMP effectors

In a previous study, we screened c-di-GMP-binding proteins in *E. coli* using a proteomic microarray and found that the rRNA

methyltransferases RlmI and RlmE were potential c-di-GMP effectors⁶ (**Fig. 1A**). Based on the demonstration of binding between c-di-GMP and the methyltransferases, we speculated that c-di-GMP might affect rRNA methylation activity. To test this hypothesis, we examined the activity of four methyltransferases in the presence of c-di-GMP, using rRNA methylation as our indicator. For this purpose, we synthesized unmethylated 23S rRNA positions 1932-1991 and 2522-2581 for m⁵C1962 by RlmI³⁵ and m²U2552 by RlmE³⁶, respectively. The methyltransferases can catalyze the production of methylated rRNA and exhibit specific peaks in HPLC (**Fig. 1B-C**). However, when c-di-GMP was introduced, methylation activities were significantly inhibited in a dose-dependent manner. We compared the effect of additional c-di-GMP on methylation products, using the group without c-di-GMP treatment as the reference value. Specifically, 5 μ M c-di-GMP inhibited the activity of RlmI and RlmE by 49% and 31%, respectively (**Fig. 1D**).

c-di-GMP inhibited ribosome assembly, with RlmI as the main effector
rRNA methylation is a prerequisite for the accurate assembly of ribosomes. We hypothesized that c-di-GMP might affect ribosomal assembly in *E. coli* (*E. coli* BW25113 as reference strain) by inhibiting methylation activity. To investigate the regulatory role of c-di-GMP, we constructed the strains of *dgcZ* knockout and overexpression. Compared

with wild-type (WT) strains, the c-di-GMP level in *dgcZ* overexpressing strains increased by 12.2 times (**Fig. S1A**). Then, we used a sucrose density gradient (SDG) assay to detect the ribosome particle, and the results showed that both knockout and overexpression of *dgcZ* could not affect the ribosome abundance of 50S compared with WT strain without antibiotic treatment (**Fig. 2A**). c-di-GMP is a stress response factor. Therefore, we hypothesized that the regulation of ribosome assembly by c-di-GMP might occur under antibiotic stress. We treated *E. coli* cells with kanamycin, a ribosome-targeted antibiotic that can also elevate the cellular c-di-GMP level in *E. coli* by increasing the mRNA levels of *dgcZ*^{6,37}. This elevation was controlled by the RNA-binding protein *csrA*^{38,39}. Following kanamycin treatment, the c-di-GMP concentrations in WT cells were 6.2-fold higher than in untreated cells (**Fig. S1A**). Notably, the c-di-GMP levels in *dgcZ*-defective cells were not responsive to kanamycin (**Fig. S1A**) because DgcZ serves as an effector for kanamycin-induced elevation of c-di-GMP levels. An SDG assay revealed that the ribosome disintegrated into 30S and 50S particles at low Mg²⁺ concentrations, and ~45S particles¹¹ were observed in kanamycin-treated WT cells and *dgcZ* replenishment strain ($\Delta dgcZ::dgcZ$) (**Fig. 2A**). However, the strain with *dgcZ* inactivation mutation did not show the presence of 45S particles ($\Delta dgcZ::dgcZ^{G206A,G207A}$). The results indicated that the increase in c-di-GMP levels inhibited the assembly of

ribosomal large subunits in *E. coli*. In addition, we found c-di-GMP inhibited the activity of four methyltransferases and downregulated the methylation of 23S RNA *in vitro* (**Fig. 1D**). Then, the four methyltransferases were overexpressed in kanamycin-treated WT cells to examine the role of the methylation enzymes in c-di-GMP-regulated ribosome assembly. We found that the overexpression of the methylases did not affect c-di-GMP levels (**Fig. S1B**), and the overexpression of RlmI weakened the effect of c-di-GMP on ribosomal assembly (**Fig. 2B**). Thus, RlmI was the major effector of c-di-GMP in regulating ribosome assembly.

c-di-GMP binds to its effectors via Arg residues⁴⁰. We mutated all Arg residues to Ala in RlmI to determine the binding sites on RlmI. Then, we developed the *in vitro* assay in which purified RlmI mutants were incubated with biotin-c-di-GMP, ultraviolet (UV)-crosslinked, and probed with fluorescent streptavidin^{41,42}. We observed that RlmI mutants with R64A and R103A exhibited a significantly weakened interaction with c-di-GMP (**Figs. 2C and S2**). Furthermore, when we determined the activity of RlmI mutants, both RlmI^{R64A} and RlmI^{R103A} displayed methylation activities slightly lower than that of RlmI under 5 μ M rRNA substrate. Upon treatment with 20 μ M c-di-GMP, the methylation activity decreased by 80%, 6%, and 32% in RlmI, RlmI^{R64A}, and RlmI^{R103A}, respectively (**Fig. 2D**). The effect of c-di-GMP for RlmI was significantly

weakened under R64A and R103A mutations in comparison to that of WT, which validated that R64 and R103 are the key sites to the binding of c-di-GMP to RlmI.

We eliminated the effect of c-di-GMP on RlmI by mutation of the binding sites R64A and R103A to validate whether RlmI was the main effector of c-di-GMP in ribosome assembly. With kanamycin treatment, WT, *rlmI*^{R64A}, *rlmI*^{R103A}, and Δ *rlmI* cells were assayed by SDG. Under kanamycin stimulation, elevated c-di-GMP in WT cells inhibited RlmI, resulting in missing rRNA methylation. This inhibition of RlmI impairs ribosomal assembly and leads to the production of 45S precursors. The *rlmI* knockout strains serve as a positive control for demonstrating *rlmI* functional defects. In addition, the R64A and R103A mutants abolished the effect of c-di-GMP on RlmI. The results showed that the ~45S particle was observed in WT and Δ *rlmI* cells but not in R64A and R103A mutants (**Fig. 2E**). Thus, RlmI played a key role in ribosomal assembly under kanamycin stress, and c-di-GMP regulated its activity.

c-di-GMP induces the closure of the catalytic pocket of RlmI

To reveal the structural mechanism of c-di-GMP regulating RlmI enzyme activity, we investigated the conformational changes of RlmI during its interaction with c-di-GMP in an aqueous ionic solution using molecular dynamics (MD) simulation. In MD simulation, root mean square

deviation (RMSD) indicated the fluctuations and stability of the conformations of RlmI and root mean square fluctuation (RMSF) revealed flexibility during the full simulation period. By RMSD and RMSF, we found that residues 160-170, 302-320, and 370-390 were mainly involved in the conformational fluctuation of RlmI (**Fig. 3A**). We labeled residues 160-170 as “Domain-I” (DM-I), residues 302-320 as “Domain-II” (DM-II), and residues 370-390 as “Domain-III” (DM-III). DM-I and DM-III are the regions of the protein that correspond to the RNA-binding area, whereas DM-II is located near the S-adenosyl-L-methionine (AdoMet) binding-related area. An overall view of the evolution of RlmI fluctuations revealed a distinct conformational fluctuation around 0.8 μ s during the simulation (average of Trajectory #1 and Trajectory #2) (**Fig. 3B**). Combining RMSD, RMSF, and trajectory analysis results, the RlmI was found to exist in two states, State-I and State-II, while interacting with c-di-GMP. c-di-GMP can interact with the RNA-binding area (State-I), and the domain DM-III shut down after 0.8 μ s. The results suggested that (1) c-di-GMP can interact with the RNA-binding domains and then induce the closure of DM-III, and (2) it was corroborated that the “on-off” of the RNA-binding area was mainly embodied by DM-III to a large extent (**Fig. 3C and Video 1-2**). The dynamic process of c-di-GMP-induced conformational rearrangements in the active domain of RlmI was similar to that of other

c-di-GMP effectors such as YcgR⁴³, FleQ⁴⁴, and CheR1⁴⁵.

R64, R103, G114, and K201 residues of RlmI interact with bound

c-di-GMP

We employed Gibbs free energy analysis to identify the dominant conformation of RlmI and c-di-GMP complex. The Gibbs free energy surfaces were shown for the two runs and their average (**Fig. 4A**), using RMSD and radius of gyration as the variables. We identified the free energy basin, the one with the lowest free energy (set to 0 kJ/mol) (**Fig. 4A, yellow point**), and found that the corresponding regions were almost overlapping for the three sets (**Fig. 4B**). Thus, the results indicated the two independent simulated trajectories as convergent and physically equivalent.

To explore the binding sites of c-di-GMP and RlmI, we superimposed the stable-state configurations of RlmI and c-di-GMP for the three sets (**Fig. 4B**). Two independent trajectories #1 and #2 were taken into consideration for the computational analysis and the average was selected for convergence and physical equivalence analysis. The average conformation showed that R64 and G114 together stabilize the guanosine moiety of c-di-GMP. Correspondingly, R103 and K201 act to stabilize the negatively charged region of c-di-GMP. It is evident that R103 and K201 formed a stable hydrogen bond with the oxygen atom of the phosphate

481 group of c-di-GMP.

482 Noncovalent interactions, including hydrogen bonds, coordination
483 bonds, and salt bridges, are crucial for maintaining the tertiary structure
484 of proteins. Benefiting from the all-atom-level precision of molecular
485 dynamics simulations, we analyzed the hydrogen bond interaction map of
486 c-di-GMP with RlmI using time-dependent atomic site distances between
487 selected atomic sites to uncover the interaction mode of c-di-GMP with
488 RlmI, providing guidance for further experimental verification. Atomic
489 detail sketches of c-di-GMP and the main residues described in this
490 section are provided in **Figures S3 and S4**. While labeling the amino acid
491 residues in the hydrogen bond interaction map of c-di-GMP with RlmI,
492 we also labeled the lifetime of hydrogen-bonding interactions between
493 c-di-GMP and corresponding amino acid residues. Considering that our
494 molecular dynamics simulation spanned a timeframe of 2 μ s, we
495 subsequently performed site mutation verification on residues with
496 hydrogen bond interaction lifetimes exceeding 400 ns. Six amino acid
497 residues from RlmI were selected as the potential binding sites for
498 c-di-GMP: R64, R103, E108, G114, T116, and K201 (**Fig. 4C**).
499 Atom-atom distances as a function of time and bond lifetimes are
500 presented in **Fig. S5-S15**.

501 We employed the streptavidin blotting assays to determine the
502 interaction between c-di-GMP and RlmI mutants, aiming to validate the

results obtained from the molecular dynamics simulations. The result revealed that amino acid residues R64, R103, G114, and K201 were crucial for the binding of c-di-GMP to the RlmI. In addition, E108A and T116A of RlmI slightly affected c-di-GMP binding (**Fig. 4D**). We next performed isothermal titration calorimetry (ITC) titrations with these mutants and determined K_d values of 1.3, 102.3, 76.5, 148.6, and 401.2 μ M for RlmI, RlmI^{R64A}, RlmI^{R103A}, RlmI^{G114A}, and RlmI^{K201A}, respectively (**Figs. 4E and S16**). We found that the stoichiometries have not significant different between RlmI and its variants, which showed 1:1 binding ratio with c-di-GMP (**Fig. 4E**). Further, we observed that the activity of RlmI^{K201A} showed no significant change with 20 μ M c-di-GMP treatment compared with c-di-GMP free group. (**Fig. 4F**). The results suggested that R64, R103, G114, and K201 residues of RlmI were the critical sites for c-di-GMP binding.

c-di-GMP regulates RlmI to promote antibiotic resistance

As a close correlation exists among c-di-GMP, ribosomal assembly, and antibiotic resistance^{46,47}, we hypothesized that c-di-GMP regulated ribosomal assembly to promote antibiotic resistance by inhibiting RlmI activity. To test this hypothesis, we interfered with the interaction of c-di-GMP and RlmI by introducing the K201 mutation in endogenous RlmI (*rlmI*^{K201A}), *dgcZ* depletion (Δ *dgcZ*), *dgcZ* overexpression (Δ *dgcZ*

dgcZ⁺) and both mutants ($\Delta dgcZ$ *rlmI*^{K201A}). Then, we determined the c-di-GMP level and methylation level of 23S rRNA C1962. The results showed that the cellular c-di-GMP levels and C1962 methylation levels did not significantly change in WT, $\Delta dgcZ$, *rlmI*^{K201A}, and $\Delta dgcZ$ *rlmI*^{K201A} without kanamycin treatment (**Figs. 5A and 5B**). However, the c-di-GMP levels of WT and *rlmI*^{K201A} increased about six times compared with $\Delta dgcZ$ and $\Delta dgcZ$ *rlmI*^{K201A} when treated by kanamycin, and the c-di-GMP levels of $\Delta dgcZ$ *dgcZ*⁺ increased about eleven times compared with WT (**Fig. 5A**). Furthermore, the methylation analysis showed that elevated c-di-GMP (WT, $\Delta dgcZ$ *dgcZ*⁺) significantly decreased C1962 methylation, and the K210A mutation (*rlmI*^{K201A}) abolished the effect of c-di-GMP (**Fig. 5B**).

We measured the growth curves and MICs of the four strains, *i.e.*, WT, $\Delta dgcZ$, *rlmI*^{K201A}, and $\Delta dgcZ$ *rlmI*^{K201A}. We tested serial concentrations (0, 1.5, 3, 6 and 9 μ g/mL) of kanamycin for strain growth curve. The strains cannot growth in treatment with 9 μ g/mL kanamycin, so we determined the growth curve for other four concentrations. The curves showed that growth of the four strains were consistent when kanamycin was not added (**Fig. 5C**). However, the growth of the $\Delta dgcZ$ strains decreased compared with that of the WT strains with 1.5, 3 and 6 μ g/mL kanamycin treatment, indicating that c-di-GMP promoted the antibiotic tolerance of *E. coli*. Furthermore, we mutated the c-di-GMP binding site K201 of RlmI

547 (*rlmI*^{K201A}) and found that *rlmI*^{K201A} strains had greater sensitivity to
548 antibiotics and slower growth rate compare to that of WT, which suggests
549 that the interaction of c-di-GMP and RlmI enhances the antibiotic
550 tolerance (**Fig. 5 C-D**).

551 Kanamycin is an antibiotic that targets ribosomes and can
552 endogenously increase the c-di-GMP level. Therefore, we speculate that
553 c-di-GMP has a promoting effect on kanamycin resistance. To test this,
554 we isolated 40 *E. coli* strains from soil (named S1-S20) and urine (named
555 C1-C20) samples resistant to kanamycin and determined the cellular
556 c-di-GMP levels to investigate the role of c-di-GMP and RlmI axis in
557 kanamycin-resistant *E. coli*. The results revealed that 13/40 strains (S3,
558 S4, S7, S12, S16, S20, C1, C2, C4, C8, C14, C15, C18) showed
559 significant increase in c-di-GMP levels compared with the BW25113
560 strains (**Fig. S17A**). Furthermore, we mutated the endogenous RlmI in
561 K201 to alanine and determined the minimal inhibitory concentration
562 (MIC). We obtained 12 of 13 K201 mutant strains, excluding the C12
563 strain, which might be a multidrug-resistant strain. Drug susceptibility
564 results showed that the MICs of the S4, S16, S20, C1 and C2 strains
565 substantially decreased following the mutation at K201 of RlmI (**Fig. 5E**).
566 Thus, c-di-GMP regulated RlmI activity to promote antibiotic tolerance,
567 and this pathway played a key role in a portion of antibiotic-resistant *E.*
568 *coli*.

569

570 *Effect of c-di-GMP on RlmI is conserved in multiple pathogenic*

571 *bacteria*

572 c-di-GMP is a ubiquitous bacterial secondary messenger, and RlmI is
 573 highly conserved in bacteria. Thus, we hypothesized that the binding and
 574 inhibition of c-di-GMP with RlmI from *E. coli* was the same for the RlmI
 575 homologues in other bacteria. RlmI protein sequences from a series of
 576 highly diverse bacteria were aligned with testing this hypothesis, and we
 577 found that the c-di-GMP binding region was reasonably well conserved in
 578 these bacteria (**Fig. 6A**). Then, we selected *Salmonella typhimurium*,
 579 *Klebsiella pneumoniae*, and *Vibrio cholerae* as the exemplary members of
 580 this conserved set. We found that RlmI^{*S. typhimurium*}, RlmI^{*K. pneumoniae*}, and
 581 RlmI^{*V. cholerae*} could bind to c-di-GMP and that the binding could be
 582 abolished when the lysine in RlmI was mutated (**Fig. 6B**). Furthermore,
 583 the *in vitro* activity analysis showed that similar to RlmI^{*E.coli*}, the
 584 aforementioned three RlmI homologues exhibited methylase activity for
 585 23S rRNA and this activity could be inhibited by c-di-GMP (**Fig. 6C**).
 586 Thus, the effect of c-di-GMP on RlmI is conserved in multiple pathogenic
 587 bacteria and might also play a role in antibiotic resistance.

588

589 **Discussion**

590 c-di-GMP is a key secondary messenger in prokaryotes. rRNA

methylation occurs in both prokaryotes and eukaryotes. This study discovered that c-di-GMP binds to four rRNA methyltransferases and inhibits their activities. RlmI was found to be the major effector of c-di-GMP in ribosome assembly. The molecular dynamics simulation analysis revealed the binding sites and models of c-di-GMP and RlmI. The MIC assay further demonstrated that c-di-GMP inhibits ribosome assembly, promoting antibiotic resistance in *E. coli*. Thus, we established a regulatory pathway among c-di-GMP and ribosome functions and revealed its role in antibiotic resistance.

Previous studies have reported that c-di-GMP regulates mature ribosome function through RimK in *Pseudomonas*^{48,49}, EF-P in *Acinetobacter baumannii*⁵⁰, Vc2 riboswitches in *V. cholerae*⁵¹. c-di-GMP regulates the glutamate ligase RimK, which catalyzes glutamate residues to the C-terminus of ribosomal protein RpsF to affect ribosomal function^{48,49}. The binding of c-di-GMP enhances the function of EF-P, promoting translation efficiency and modulating bacterial physiology and virulence⁵⁰. Additionally, c-di-GMP binds to the Vc2 riboswitch, inducing structural changes that result in the switch-OFF and switch-ON states of translational initiation⁵¹. This study revealed that c-di-GMP affects ribosome assembly, offering a new perspective on c-di-GMP's role in ribosome regulation. Numerous accessory factors play a role in guiding the ribosome assembly process, including GTPases, rRNA

613 modification enzymes, helicases, and maturation factors⁵². Our findings
614 establish c-di-GMP as an upstream regulatory signal for rRNA
615 modification, creating a connection between environmental stimuli and
616 ribosome function.

617 RlmI is a large ribosomal RNA subunit methyltransferase that
618 methylates cytosine specifically at position 1962 (m⁵C1962) of 23S
619 rRNA. In previous studies, RlmI depletion did not lead to abnormal
620 ribosome assembly or growth arrest of *E. coli* at 20°C and 37°C⁵³. Indeed,
621 we found that RlmI depletion did not affect the ribosome abundance of
622 50S compared with WT strains when not treated with antibiotics.

623 However, with kanamycin treatment, the ~45S particle was observed in
624 $\Delta rlmI$ cells (**Fig. 2E**). Thus, RlmI plays a key role in ribosomal assembly
625 under kanamycin stress. As deletion of most ribosomal
626 methyltransferases does not cause significant phenotypic changes, these
627 studies have demonstrated that the function of methylases under different
628 growth conditions may help understand the physiological significance of
629 ribosome assembly.

630 rRNA methylation is a fundamental mechanism contributing to
631 bacterial resistance against ribosome-targeting antibiotics. Genes
632 encoding corresponding methyltransferases have been identified in
633 clinical isolates of pathogenic bacteria⁵⁴. In 16S rRNA, methylation of
634 C1405 and A1408 confer high-level resistance to aminoglycosides, which

is catalyzed by the RsmF and Npm families, respectively. The phylogenetic analysis suggests that m⁷G1405 and m¹A1408 methyltransferases share a common ancestor with aminoglycoside-producing soil bacteria. In 23S rRNA, the SAM methyltransferase family shares ancestry with the housekeeping RlmN methyltransferases, which incorporate the methylation of A2503 in 23S rRNA. However, the connection between RlmI and antibiotic resistance has not previously been reported. We also detected the transcriptional levels of RlmI for the drug-resistant strains and did not find any intrinsic change in expression levels (**Fig. S17B**). Because RlmI is not the direct target of most of the known antibiotics, and its enzymatic activity could be regulated through the binding of c-di-GMP. We speculate that RlmI may function as an effector of the stress factor c-di-GMP, and the pathway of c-di-GMP regulating RlmI may play the role in intrinsic tolerance.

Bacteria mainly acquire resistance by altering resistance genes, reducing intracellular antibiotic concentrations, protecting antibiotic targets, and inactivating antibiotics⁵⁵. c-di-GMP promotes the biofilm to reduce the permeability of antibiotics^{46,56}. Other mechanisms by which c-di-GMP promotes bacterial resistance remain to be studied. We found that the level of c-di-GMP increased in some drug-resistant *E. coli* and interfering with the effect of c-di-GMP on ribosome methylation in these

bacteria could increase their sensitivity to antibiotics. c-di-GMP has essential physiological functions in drug-resistant bacteria. However, not all drug-resistant bacteria have elevated intracellular c-di-GMP concentrations, and c-di-GMP regulates other drug-resistance-related pathways, such as biofilms. The question of whether the resistance pathway regulated by c-di-GMP has a synergistic or independent effect is worth exploring. Therefore, more data on drug-resistant strains are needed to examine the role of c-di-GMP in bacterial resistance.

In summary, we identified rRNA methyltransferases as the novel c-di-GMP effectors from *E. coli* proteome microarray assay. The functional analysis revealed an unexpected role of c-di-GMP in regulating ribosome assembly by inhibiting rRNA methylases, highlighting the physiological function of the regulatory axis in bacterial drug resistance.

Acknowledgments

This study was supported by the National Natural Science Foundation of China (Grant No. 32000027), the Natural Science Foundation of Fujian Province, China (No. 2022J01197), Fourteenth Five-Year National Key Research and Development Program of China (2023YFC2307200), R&D Program of Guangzhou National Laboratory (No. GZNL2023A01005) and Natural Science Foundation of China (No. 92374110).

Author contributions

Z.W.X., S.C.T. and J.M. conceived the idea. S.C.T. provided key reagent. S.Q.Y., X.R.L., J.Y.S., and H.C. performed protein mutation and interaction assay. X.T.X. performed the bacterial culture and protein purification. S.Q.Y., M.L., and X.T.X. performed an enzyme activity assay. X.T.X., X.R.L., X.T.X., and L.X.Z. performed the bacterial drug sensitivity test. Z.Y.H. and J.M. performed molecular dynamic simulation and structure analysis. Z.W.X., S.Q.Y., Z.Y.H., and J.M. prepared the figures. Z.W.X., S.Q.Y., Z.Y.H., and J.M. wrote the manuscript.

Data and software availability

The crystal structure files, MD simulation files (input files, parameter files, topology files, etc.), and structures of c-di-GMP are available on the website <https://github.com/Zheyao-Hu/RlmIcdiGMP>. Moreover, all the software (free to use) packages used in this study were the official release version without any modification. The raw protein microarray data have been published in the Protein Microarray Database (www.proteinmicroarray.cn/) with the accession number PMDE226 (http://www.proteinmicroarray.cn/index.php/experiment/detail?experiment_id=226).

Conflicts of interest

The authors declare no conflicts of interest.

Figure legends

Figure 1. Ribosomal RNA large subunit methyltransferases are c-di-GMP effectors.

(A) *E. coli* proteome microarrays were probed with biotin-c-di-GMP and biotin. Obvious binding differences of RlmI and RlmE on the microarrays incubated with biotin-c-di-GMP and biotin were observed. Two spots per protein were observed, and the positive signal-to-noise ratio [(SNR) (+)] represented the average SNR of the two duplicate spots. (B-C) *In vitro* methylation reaction. The synthesized rRNA fragments were used for *in vitro* methylation enzyme activity testing. The HPLC peaks are derived from RlmI (B) and RlmE (C) with the treatment of 0, 5, 10 and 20 μ M c-di-GMP, respectively. (D) Quantitative results of HPLC peak. The methylated rRNAs were detected by HPLC and quantified by area under the curve. The bar chart shows the relative enzyme activity with the data points, using the reaction without the addition of c-di-GMP as the baseline (three preparations, mean \pm range; $**p < 0.01$, two-tailed Student's t-test).

Figure 2. c-di-GMP inhibits ribosome assembly, with RlmI as the main effector.

(A) SDG assay for the strains with elevated c-di-GMP. c-di-GMP was

723 elevated by treatment with kanamycin or overexpression of DgcZ, and
724 the ribosome particle was assayed by SDG. The corresponding three
725 peaks represent the ribosome particles of 30S, pre-50S, and 50S. (B) SDG
726 assay for the strains overexpressing two methyltransferases. RlmI and
727 RlmE were overexpressed under the conditions of kanamycin treatment,
728 and the ribosome particle was assayed by SDG. (C) Streptavidin blotting
729 assays for WT and mutant RlmI. The arginine on RlmI was mutated to
730 alanine, and the interaction of c-di-GMP and RlmI mutants was
731 determined. The results indicated that R64A and R103A weakened the
732 binding of c-di-GMP and RlmI. Streptavidin represents the interaction
733 signals, and α -His represents the protein levels. The bar chart shows the
734 relative intensity of streptavidin with the data points (three preparations,
735 mean \pm range; $**p < 0.01$, two-tailed Student's t-test). (D) *In vitro*
736 methylation assay of the two RlmI mutants. The synthesized rRNA
737 fragments were used as substrates, and the reaction products were
738 analyzed by HPLC. The bar chart shows the relative activity of RlmI with
739 the data points (three preparations, mean \pm range; ns: no significant
740 difference, $*p < 0.05$, $**p < 0.01$, two-tailed Student's t-test). (E) SDG
741 assay for the strains with RlmI depletion and mutation. Strains with
742 endogenous depletion and mutation of RlmI were constructed using the
743 Red-recombination system. These strains were treated with kanamycin,
744 and the ribosome particle was assayed by SDG.

Figure 3. Binding model of c-di-GMP and RlmI.

(A) RMSD value of RlmI during interaction with c-di-GMPs. The arrow marks the main changes at the residue level. The solid and dashed lines represent two simulated trajectories, and the degree of overlap represents the convergence of two trajectories. (B) RMSF value of RlmI during interaction with c-di-GMP. The arrow marks the main changes on the timeline. (C) Representative snapshots of the transition between RlmI State-I and State-II. The arrow marks the main changes in DM-III.

Figure 4. Determination of the binding sites of c-di-GMP on RlmI.

(A) Gibbs free energy landscapes illustrating the binding of c-di-GMP to RlmI. I#1, I#2, and I represent trajectories 1, 2, and average, respectively. (B) Interaction model of c-di-GMP and RlmI. The key binding sites R64, R103, G114, and K201 are highlighted. I#1, I#2, and I represent trajectories 1, 2, and average, respectively. (C) Interaction landscapes of c-di-GMP and RlmI. The interaction sites between c-di-GMP and RlmI in MD simulation are marked in the plane diagram of c-di-GMP. The annotated duration represents the interaction time between c-di-GMP and RlmI in the 10 μ s MD simulation, with green boxes highlighting residues with interaction times greater than 400 ns. (D) Streptavidin blotting assays comparing WT and mutant RlmI. The potential binding sites within RlmI were mutated to alanine, and the interaction with c-di-GMP was determined. Streptavidin represents the interaction signals, and α -His

represents the protein levels. The intensity of WT was used as the reference for statistical analysis of the variants. The bar chart shows the relative intensity of streptavidin with the data points (three preparations, mean \pm range; * $p < 0.05$, ** $p < 0.01$, two-tailed Student's t-test). (E) ITC analysis of the binding between c-di-GMP and RlmI. c-di-GMP was titrated into RlmI and its mutants by three repetitions. (F) *In vitro* methylation assay of the RlmI mutants. The bar chart shows the relative activity of RlmI with the data points (three preparations, mean \pm range; ns: no significant difference, two-tailed Student's t-test).

Figure 5. c-di-GMP regulates ribosome assembly to promote drug resistance.

(A) Relative c-di-GMP level of WT, $\Delta dgcZ$, $\Delta dgcZ dgcZ^+$, $rlmI^{K201A}$ and $\Delta dgcZ rlmI^{K201A}$ strains. The intracellular c-di-GMP concentrations were determined by UPLC-IM-MS. The bar chart shows the relative quantification of c-di-GMP with the data points (three preparations, mean \pm range; ** $p < 0.01$, two-tailed Student's t-test). (B) Methylation level of C1962 in 23S rRNA of WT, $\Delta dgcZ$, $\Delta dgcZ dgcZ^+$, $rlmI^{K201A}$ and $\Delta dgcZ rlmI^{K201A}$ strains. The endogenous methylation level in C1962 was determined by meRIP-qPCR in triplicate. The bar chart shows the relative quantification of methylated rRNA with the data points. (C) Growth curves of the WT, $\Delta dgcZ$, $rlmI^{K201A}$ and $\Delta dgcZ rlmI^{K201A}$ strains. The *E. coli* strains were cultured in Vogel-Bonner medium with 0, 1.5, 3 and 6

789 $\mu\text{g/mL}$ kanamycin treatment, respectively. The growth was measured after
 790 8, 12, 16, 20, 24, and 32 h in triplicate (three preparations, mean \pm range).
 791 (D) The MICs for the WT, $\Delta dgcZ$, $rlmI^{K201A}$ and $\Delta dgcZ rlmI^{K201A}$ strains.
 792 The bar chart shows the MICs, which were determined by ETEST. The
 793 bar chart shows the value of MICs with the data points (three preparations,
 794 mean \pm range; ns: no significant difference, $**p < 0.01$, two-tailed
 795 Student's t-test). (E) The MICs of the resistant strains. The 12
 796 kanamycin-resistant strains were mutated from RlmI K210 to alanine, and
 797 the MICs were determined by ETEST. The fold changes of MIC
 798 ($\text{MIC}_{rlmI^{K201A}}/\text{MIC}_{WT}$) were annotated for the strains with
 799 statistically different MICs upon the mutation of K201 to Alanine. The
 800 bar chart shows the value of MICs with the data points (three preparations,
 801 mean \pm range; $*p < 0.05$, $**p < 0.01$, two-tailed Student's t-test).

802 **Figure 6. c-di-GMP binds RlmI and inhibits its activity conserved in**
 803 **multiple pathogenic bacteria.**

804 (A) CLUSTALW alignment of the binding sites of c-di-GMP and RlmI.
 805 Residues involved in c-di-GMP binding (R64, R103, G114, and K201)
 806 are marked by red arrows. (B) Streptavidin blotting assays for RlmI of
 807 four species. The WT and mutant RlmI interacted with biotin-c-di-GMP
 808 and were crosslinked by UV. Streptavidin and α -His present interaction
 809 signals and protein levels, respectively. (C) *In vitro* methylation assay for
 810 the RlmI of four species. The experiment was performed in triplicate. The

bar chart shows the quantitative results of methylation products with the data points (three preparations, mean \pm range; ns: no significant difference, $*p < 0.05$, $**p < 0.01$, two-tailed Student's t-test).

References

- 1 ROSS, P. *et al.* Regulation of cellulose synthesis in *Acetobacter xylinum* by cyclic diguanylic acid. *Nature* **325**, 279-281, doi:10.1038/325279a0 (1987).
- 2 Hengge, R. Principles of c-di-GMP signalling in bacteria. *Nature reviews. Microbiology* **7**, 263-273, doi:10.1038/nrmicro2109 (2009).
- 3 Jenal, U., Reinders, A. & Lori, C. Cyclic di-GMP: second messenger extraordinaire. *Nature reviews. Microbiology*, doi:10.1038/nrmicro.2016.190 (2017).
- 4 Romling, U., Galperin, M. Y. & Gomelsky, M. Cyclic di-GMP: the First 25 Years of a Universal Bacterial Second Messenger. *Microbiology and Molecular Biology Reviews* **77**, 1-52, doi:10.1128/mmbr.00043-12 (2013).
- 5 Obeng, N. *et al.* Bacterial c-di-GMP has a key role in establishing host-microbe symbiosis. *Nature microbiology*, doi:10.1038/s41564-023-01468-x (2023).
- 6 Xu, Z. *et al.* Interplay between the bacterial protein deacetylase CobB and the second messenger c-di-GMP. *The EMBO journal* **38**, e100948, doi:10.15252/emj.2018100948 (2019).
- 7 Arai, T., Ishiguro, K., Kimura, S., Sakaguchi, Y. & Suzuki, T. Single methylation of 23S rRNA triggers late steps of 50S ribosomal subunit assembly. *Proceedings of the National Academy of Sciences of the United States of America* **112**, E4707-4716, doi:10.1073/pnas.1506749112 (2015).

833 8 Connolly, K., Rife, J. P. & Culver, G. Mechanistic insight into the ribosome biogenesis
834 functions of the ancient protein KsgA. *Molecular microbiology* **70**, 1062-1075,
835 doi:10.1111/j.1365-2958.2008.06485.x (2008).

836 9 Champney, S. Macromolecular Structure Assembly as a Novel Antibiotic Target.
837 *Antibiotics* **11**, doi:10.3390/antibiotics11070937 (2022).

838 10 Champney, W. S. Antibiotics targeting bacterial ribosomal subunit biogenesis. *Journal*
839 *of Antimicrobial Chemotherapy* **75**, 787-806, doi:10.1093/jac/dkz544 (2020).

840 11 Corrigan, R. M., Bellows, L. E., Wood, A. & Grundling, A. ppGpp negatively impacts
841 ribosome assembly affecting growth and antimicrobial tolerance in Gram-positive
842 bacteria. *Proceedings of the National Academy of Sciences of the United States of*
843 *America* **113**, E1710-1719, doi:10.1073/pnas.1522179113 (2016).

844 12 Zhang, Y. E. *et al.* (p)ppGpp Regulates a Bacterial Nucleosidase by an Allosteric
845 Two-Domain Switch. *Molecular cell* **74**, 1239-1249 e1234,
846 doi:10.1016/j.molcel.2019.03.035 (2019).

847 13 Wang, B., Grant, R. A. & Laub, M. T. ppGpp Coordinates Nucleotide and Amino-Acid
848 Synthesis in *E. coli* During Starvation. *Molecular cell* **80**, 29-42.e10,
849 doi:10.1016/j.molcel.2020.08.005 (2020).

850 14 Jeremia, L., Deprez, B. E., Dey, D., Conn, G. L. & Wuest, W. M. Ribosome-targeting
851 antibiotics and resistance via ribosomal RNA methylation. *RSC Medicinal Chemistry*
852 **14**, 624-643, doi:10.1039/d2md00459c (2023).

853 15 Gutierrez, B. *et al.* Fitness Cost and Interference of Arm/Rmt Aminoglycoside
854 Resistance with the RsmF Housekeeping Methyltransferases. *Antimicrobial Agents*

855 *and Chemotherapy* **56**, 2335-2341, doi:10.1128/aac.06066-11 (2012).

856 16 Wachino, J.-i. *et al.* Novel Plasmid-Mediated 16S rRNA m1A1408 Methyltransferase,
857 NpmA, Found in a Clinically Isolated Escherichia coli Strain Resistant to Structurally
858 Diverse Aminoglycosides. *Antimicrobial Agents and Chemotherapy* **51**, 4401-4409,
859 doi:10.1128/aac.00926-07 (2007).

860 17 Griffith, L. J., Ostrander, W. E., Mullins, C. G. & Beswick, D. E. Drug Antagonism
861 between Lincomycin and Erythromycin. *Science* **147**, 746-747,
862 doi:10.1126/science.147.3659.746 (1965).

863 18 Greninger, A. L. *et al.* International Spread of Multidrug-Resistant Campylobacter coli
864 in Men Who Have Sex With Men in Washington State and Québec, 2015–2018.
865 *Clinical Infectious Diseases* **71**, 1896-1904, doi:10.1093/cid/ciz1060 (2020).

866 19 Krüger, H. *et al.* Novel macrolide-lincosamide-streptogramin B resistance gene
867 erm(54) in MRSA ST398 from Germany. *Journal of Antimicrobial Chemotherapy* **77**,
868 2296-2298, doi:10.1093/jac/dkac149 (2022).

869 20 Schwarz, S., Werckenthin, C. & Kehrenberg, C. Identification of a Plasmid-Borne
870 Chloramphenicol-Florfenicol Resistance Gene in Staphylococcus sciuri. *Antimicrobial*
871 *Agents and Chemotherapy* **44**, 2530-2533, doi:10.1128/aac.44.9.2530-2533.2000
872 (2000).

873 21 Yan, F. *et al.* RlmN and Cfr are Radical SAM Enzymes Involved in Methylation of
874 Ribosomal RNA. *Journal of the American Chemical Society* **132**, 3953-3964,
875 doi:10.1021/ja910850y (2010).

876 22 Poteete, A. R. What makes the bacteriophage lambda Red system useful for genetic

877 engineering: molecular mechanism and biological function. *FEMS Microbiol. Lett.* **201**,
878 9-14, doi:10.1016/s0378-1097(01)00242-7 (2001).

879 23 Tu, S. *et al.* YcgC represents a new protein deacetylase family in prokaryotes. *Elife* **4**,
880 doi:10.7554/eLife.05322.00110.7554/eLife.05322.002 (2015).

881 24 Daan Frenkel & Smit., B. *Understanding molecular simulation: from algorithms to*
882 *applications*. Vol. 1 (Elsevier, 2001).

883 25 Marrink, S. J. *et al.* Computational Modeling of Realistic Cell Membranes. *Chemical*
884 *Reviews* **119**, 6184-6226, doi:10.1021/acs.chemrev.8b00460 (2019).

885 26 Nagy, G., Gordillo, M. C., Guàrdia, E. & Martí, J. Liquid Water Confined in Carbon
886 Nanochannels at High Temperatures. *The Journal of Physical Chemistry B* **111**,
887 12524-12530, doi:10.1021/jp073193m (2007).

888 27 Calero, C., Martí, J. & Guàrdia, E. 1H Nuclear Spin Relaxation of Liquid Water from
889 Molecular Dynamics Simulations. *The Journal of Physical Chemistry B* **119**,
890 1966-1973, doi:10.1021/jp510013q (2015).

891 28 Jo, S., Kim, T., Iyer, V. G. & Im, W. CHARMM-GUI: a web-based graphical user
892 interface for CHARMM. *J Comput Chem* **29**, 1859-1865, doi:10.1002/jcc.20945
893 (2008).

894 29 Kern, N. R., Lee, J., Kyo Choi, Y. & Im, W. CHARMM-GUI multicomponent assembler
895 for modeling and simulation of complex multicomponent systems. *Biophysical Journal*
896 **121**, doi:10.1016/j.bpj.2021.11.2789 (2022).

897 30 Huang, J. & MacKerell, A. D. CHARMM36 all-atom additive protein force field:
898 Validation based on comparison to NMR data. *Journal of Computational Chemistry* **34**,

899 2135-2145, doi:10.1002/jcc.23354 (2013).

900 31 Berendsen, H. J. C., van der Spoel, D. & van Drunen, R. GROMACS: A
901 message-passing parallel molecular dynamics implementation. *Computer Physics*
902 *Communications* **91**, 43-56, doi:10.1016/0010-4655(95)00042-e (1995).

903 32 Humphrey, W., Dalke, A. & Schulten, K. VMD: Visual molecular dynamics. *Journal of*
904 *Molecular Graphics* **14**, 33-38, doi:10.1016/0263-7855(96)00018-5 (1996).

905 33 Pettersen, E. F. *et al.* UCSF Chimera?A visualization system for exploratory research
906 and analysis. *Journal of Computational Chemistry* **25**, 1605-1612,
907 doi:10.1002/jcc.20084 (2004).

908 34 Spangler, C., Bohm, A., Jenal, U., Seifert, R. & Kaeffer, V. A liquid
909 chromatography-coupled tandem mass spectrometry method for quantitation of cyclic
910 di-guanosine monophosphate. *Journal of microbiological methods* **81**, 226-231,
911 doi:10.1016/j.mimet.2010.03.020 (2010).

912 35 Purta, E., O'Connor, M., Bujnicki, J. M. & Douthwaite, S. YccW is the m5C
913 Methyltransferase Specific for 23S rRNA Nucleotide 1962. *J. Mol. Biol.* **383**, 641-651,
914 doi:10.1016/j.jmb.2008.08.061 (2008).

915 36 Caldas, T. *et al.* The FtsJ/RrmJ Heat Shock Protein of Escherichia coli Is a 23 S
916 Ribosomal RNA Methyltransferase. *J. Biol. Chem.* **275**, 16414-16419,
917 doi:10.1074/jbc.M001854200 (2000).

918 37 Ho, C. L. *et al.* Visualizing the perturbation of cellular cyclic di-GMP levels in bacterial
919 cells. *Journal of the American Chemical Society* **135**, 566-569, doi:10.1021/ja310497x
920 (2013).

921 38 Lacanna, E., Bigosch, C., Kaefer, V., Boehm, A. & Becker, A. Evidence for
922 Escherichia coli Diguanylate Cyclase DgcZ Interlinking Surface Sensing and Adhesion
923 via Multiple Regulatory Routes. *Journal of bacteriology* **198**, 2524-2535,
924 doi:10.1128/JB.00320-16 (2016).

925 39 Boehm, A. *et al.* Second messenger signalling governs Escherichia coli biofilm
926 induction upon ribosomal stress. *Molecular microbiology* **72**, 1500-1516,
927 doi:10.1111/j.1365-2958.2009.06739.x (2009).

928 40 Chou, S. H. & Galperin, M. Y. Diversity of Cyclic Di-GMP-Binding Proteins and
929 Mechanisms. *Journal of bacteriology* **198**, 32-46, doi:10.1128/JB.00333-15 (2016).

930 41 Kramer, K. *et al.* Photo-cross-linking and high-resolution mass spectrometry for
931 assignment of RNA-binding sites in RNA-binding proteins. *Nature methods* **11**,
932 1064-1070, doi:10.1038/nmeth.3092 (2014).

933 42 Shu, C., Yi, G., Watts, T., Kao, C. C. & Li, P. Structure of STING bound to cyclic
934 di-GMP reveals the mechanism of cyclic dinucleotide recognition by the immune
935 system. *Nature structural & molecular biology* **19**, 722-724, doi:10.1038/nsmb.2331
936 (2012).

937 43 Hou, Y.-J. *et al.* Structural insights into the mechanism of c-di-GMP-bound YcgR
938 regulating flagellar motility in Escherichia coli. *Journal of Biological Chemistry* **295**,
939 808-821, doi:10.1016/s0021-9258(17)49937-6 (2020).

940 44 Matsuyama, B. Y. *et al.* Mechanistic insights into c-di-GMP-dependent control of the
941 biofilm regulator FleQ from Pseudomonas aeruginosa. *Proceedings of the National*
942 *Academy of Sciences* **113**, doi:10.1073/pnas.1523148113 (2015).

943 45 Yan, X.-F. *et al.* Structural analyses unravel the molecular mechanism of cyclic
944 di-GMP regulation of bacterial chemotaxis via a PilZ adaptor protein. *Journal of*
945 *Biological Chemistry* **293**, 100-111, doi:10.1074/jbc.M117.815704 (2018).

946 46 Gupta, K., Liao, J., Petrova, O. E., Cherny, K. E. & Sauer, K. Elevated levels of the
947 second messenger c-di-GMP contribute to antimicrobial resistance of *Pseudomonas*
948 *aeruginosa*. *Molecular microbiology* **92**, 488-506, doi:10.1111/mmi.12587 (2014).

949 47 Gomez, J. E. *et al.* Ribosomal mutations promote the evolution of antibiotic resistance
950 in a multidrug environment. *Elife* **6**, doi:10.7554/eLife.20420 (2017).

951 48 Hayes, C. S. *et al.* Adaptive Remodeling of the Bacterial Proteome by Specific
952 Ribosomal Modification Regulates *Pseudomonas* Infection and Niche Colonisation.
953 *PLoS genetics* **12**, doi:10.1371/journal.pgen.1005837 (2016).

954 49 Sogaard-Andersen, L. *et al.* Control of mRNA translation by dynamic ribosome
955 modification. *PLoS genetics* **16**, doi:10.1371/journal.pgen.1008837 (2020).

956 50 Guo, Q. *et al.* Elongation factor P modulates *Acinetobacter baumannii* physiology and
957 virulence as a cyclic dimeric guanosine monophosphate effector. *Proceedings of the*
958 *National Academy of Sciences* **119**, doi:10.1073/pnas.2209838119 (2022).

959 51 Inuzuka, S. *et al.* Recognition of cyclic-di-GMP by a riboswitch conducts translational
960 repression through masking the ribosome-binding site distant from the aptamer
961 domain. *Genes to Cells* **23**, 435-447, doi:10.1111/gtc.12586 (2018).

962 52 Davis, J. H. & Williamson, J. R. Structure and dynamics of bacterial ribosome
963 biogenesis. *Philosophical Transactions of the Royal Society B: Biological Sciences*
964 **372**, doi:10.1098/rstb.2016.0181 (2017).

965 53 Pletnev, P. *et al.* Comprehensive Functional Analysis of Escherichia coli Ribosomal
966 RNA Methyltransferases. *Frontiers in Genetics* **11**, doi:10.3389/fgene.2020.00097
967 (2020).

968 54 Osterman, I. A., Dontsova, O. A. & Sergiev, P. V. rRNA Methylation and Antibiotic
969 Resistance. *Biochemistry (Moscow)* **85**, 1335-1349, doi:10.1134/s000629792011005x
970 (2020).

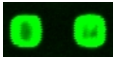



971 55 Blair, J. M., Webber, M. A., Baylay, A. J., Ogbolu, D. O. & Piddock, L. J. Molecular
972 mechanisms of antibiotic resistance. *Nature reviews. Microbiology* **13**, 42-51,
973 doi:10.1038/nrmicro3380 (2015).

974 56 Darby, E. M. *et al.* Molecular mechanisms of antibiotic resistance revisited. *Nature*
975 *Reviews Microbiology* **21**, 280-295, doi:10.1038/s41579-022-00820-y (2022).

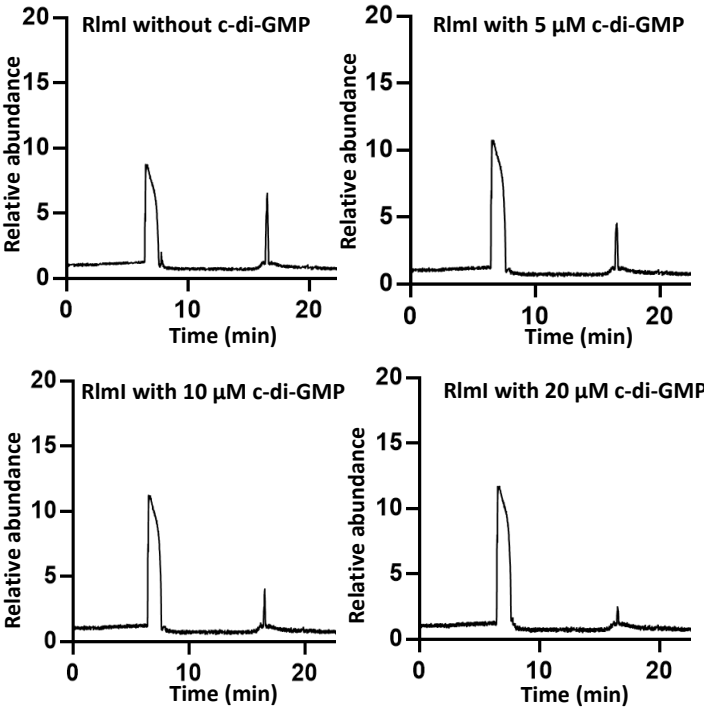
976

Figure 1

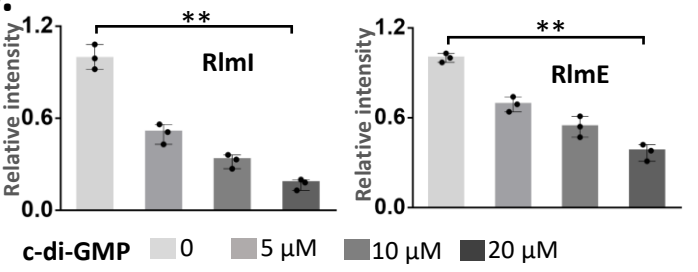
A.

Protein	Bio-c-di-GMP	Biotin	SNR(+)	P value
RImI			2.63	2.41×10^{-7}
RImE			2.25	8.63×10^{-7}

B.



D.



C.

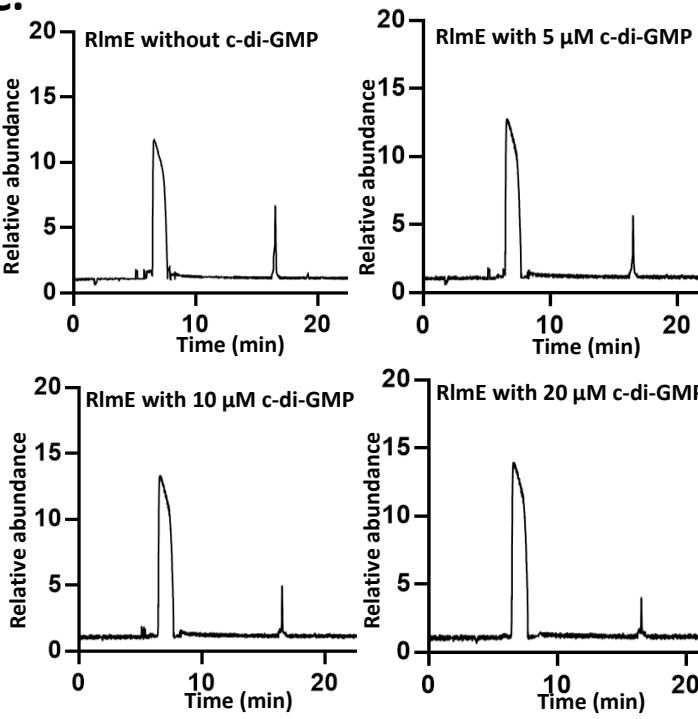


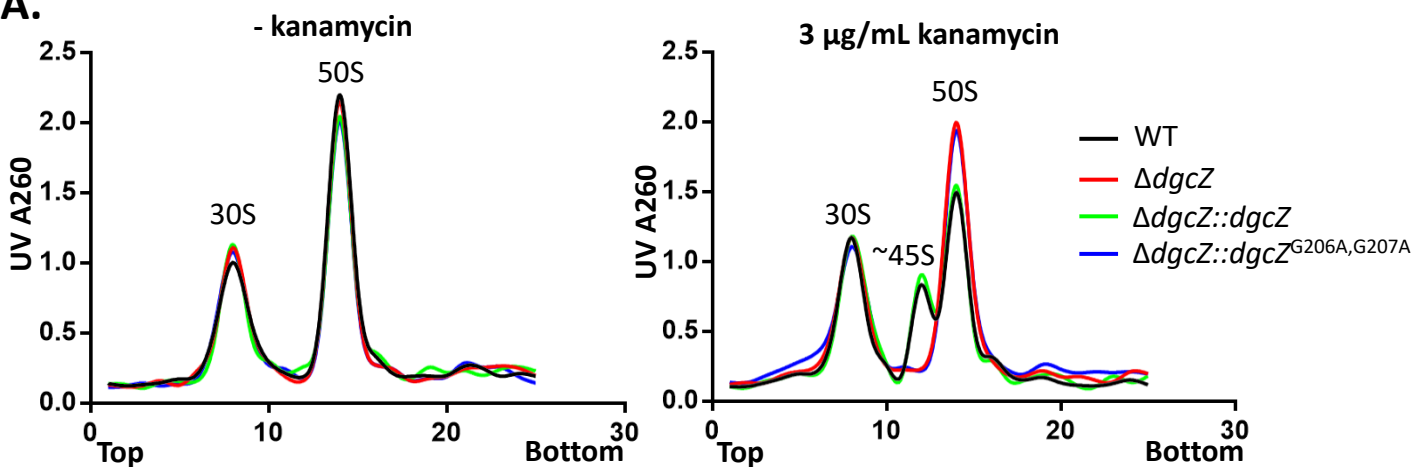
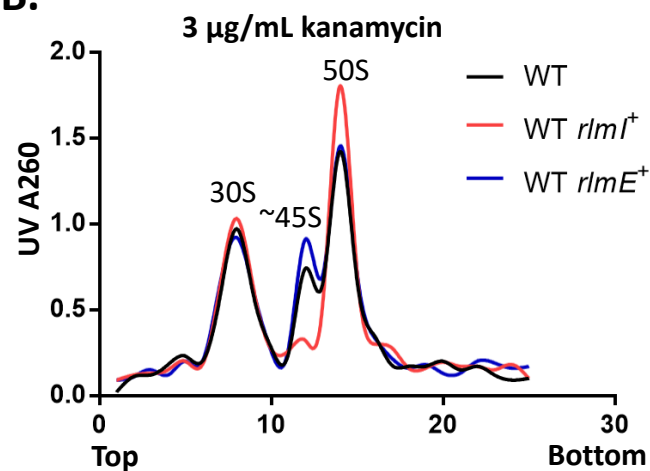
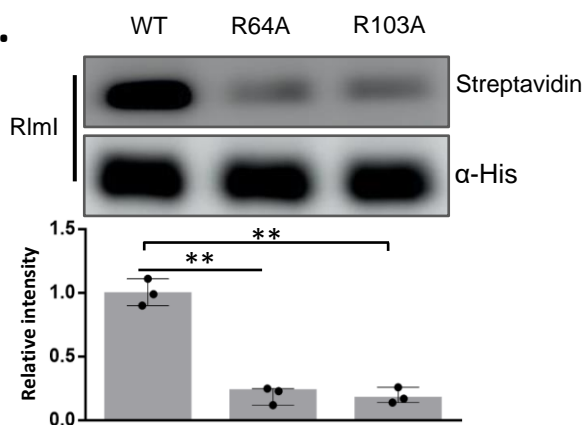
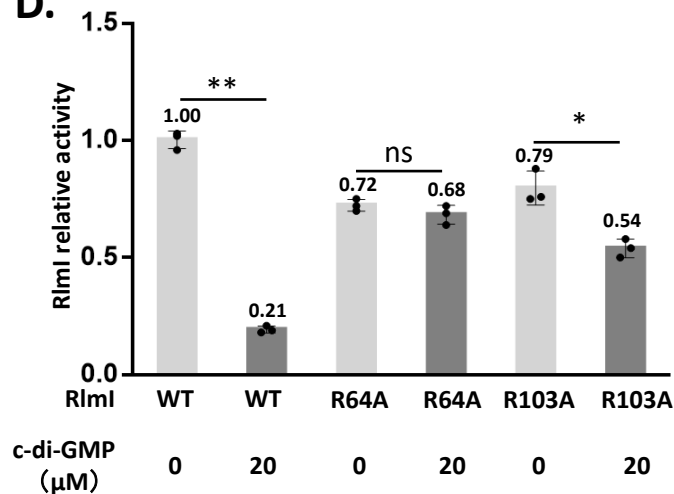
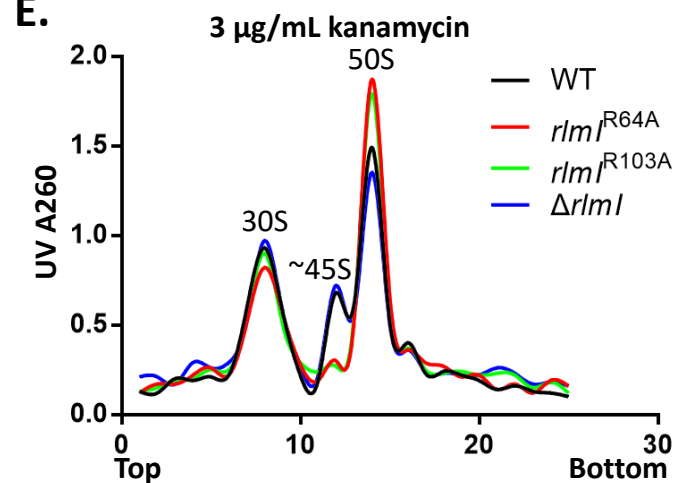
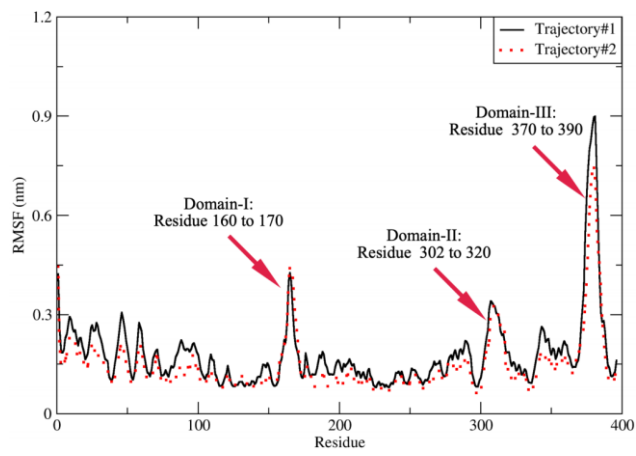
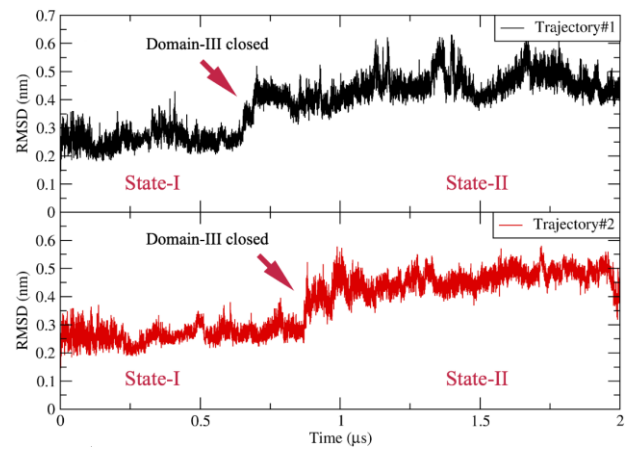
Figure 2**A.****B.****C.****D.****E.**

Figure 3

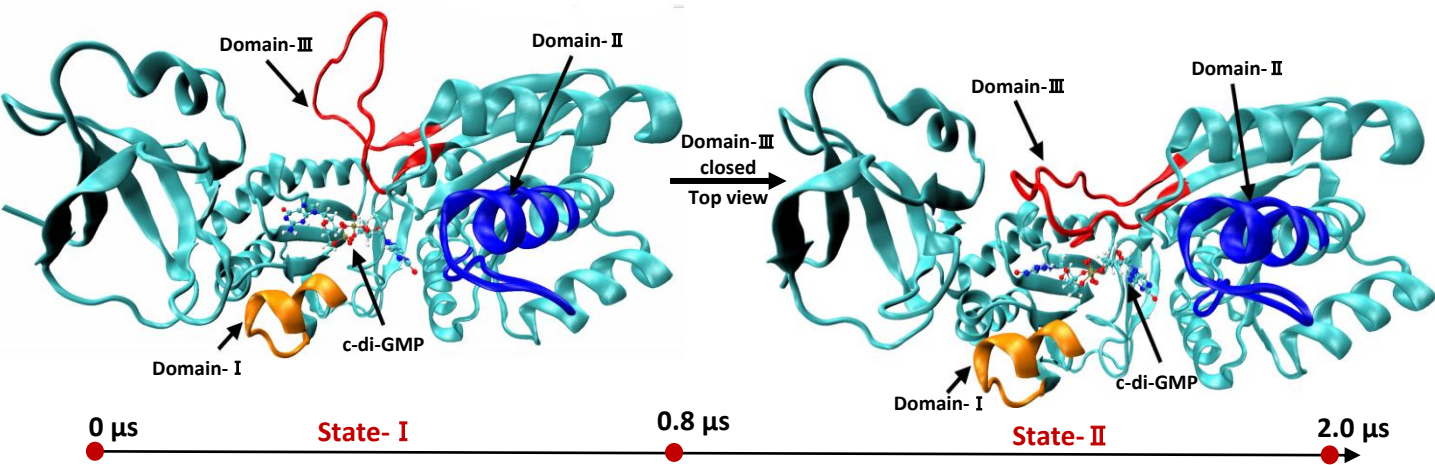
A.



B.



C.



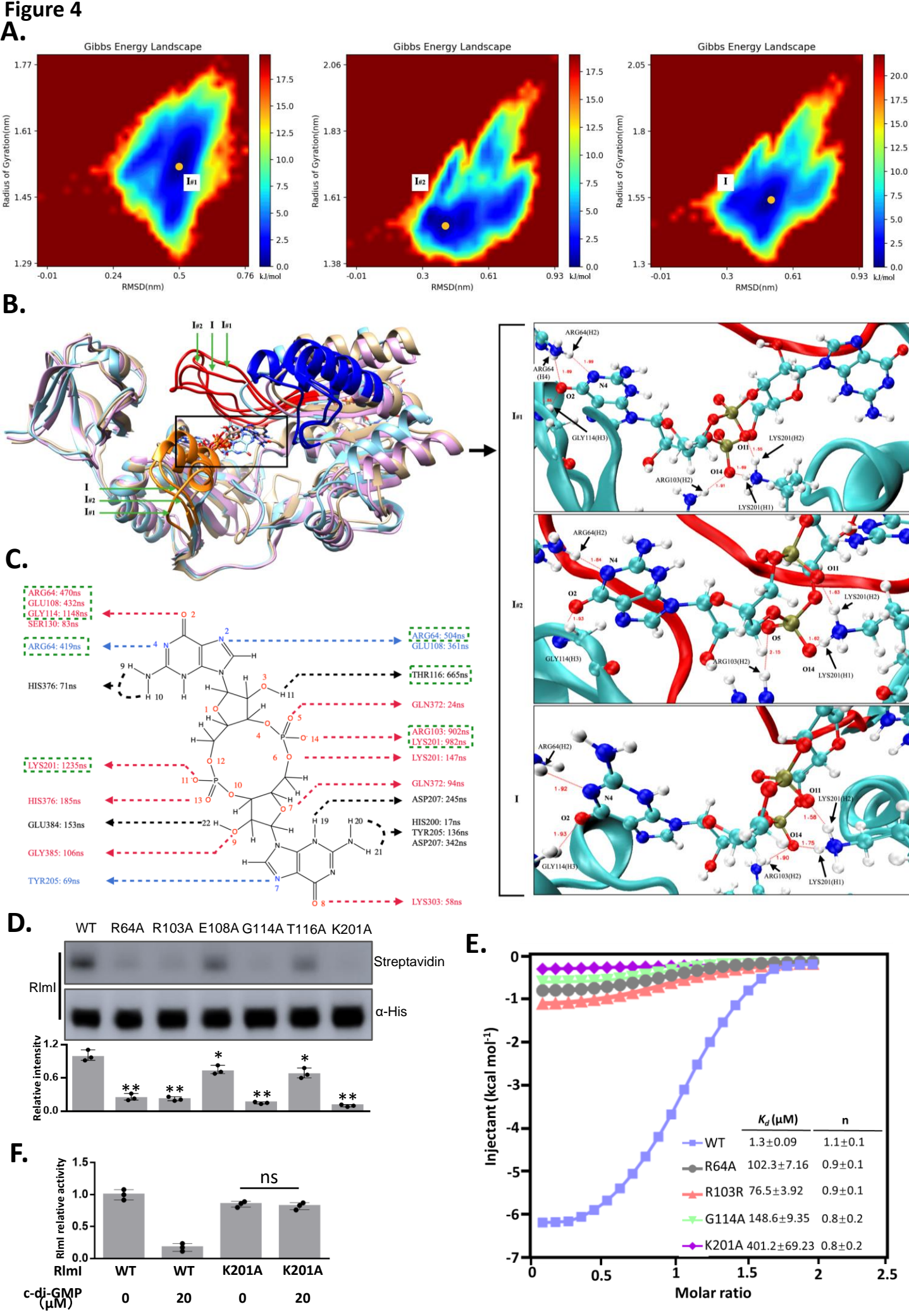


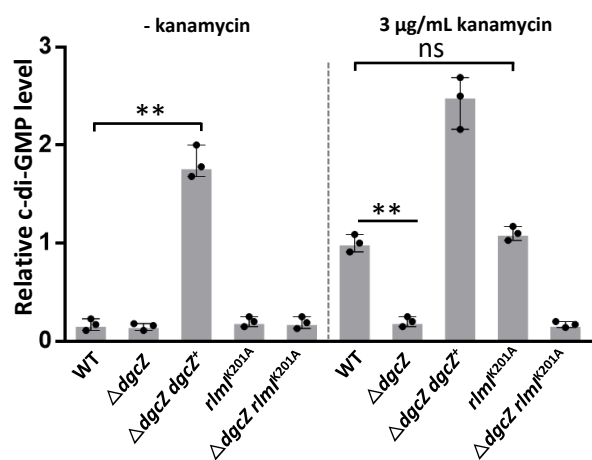
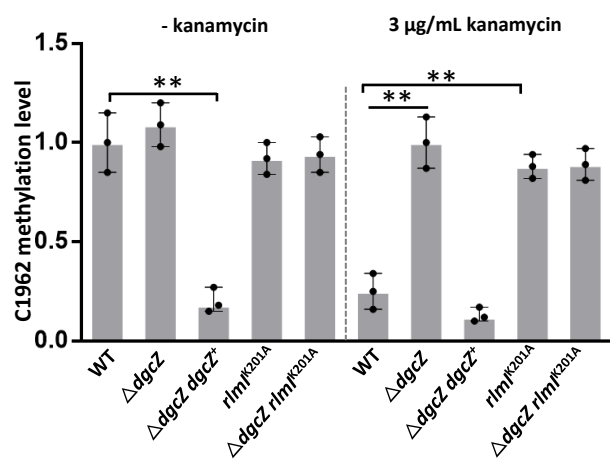
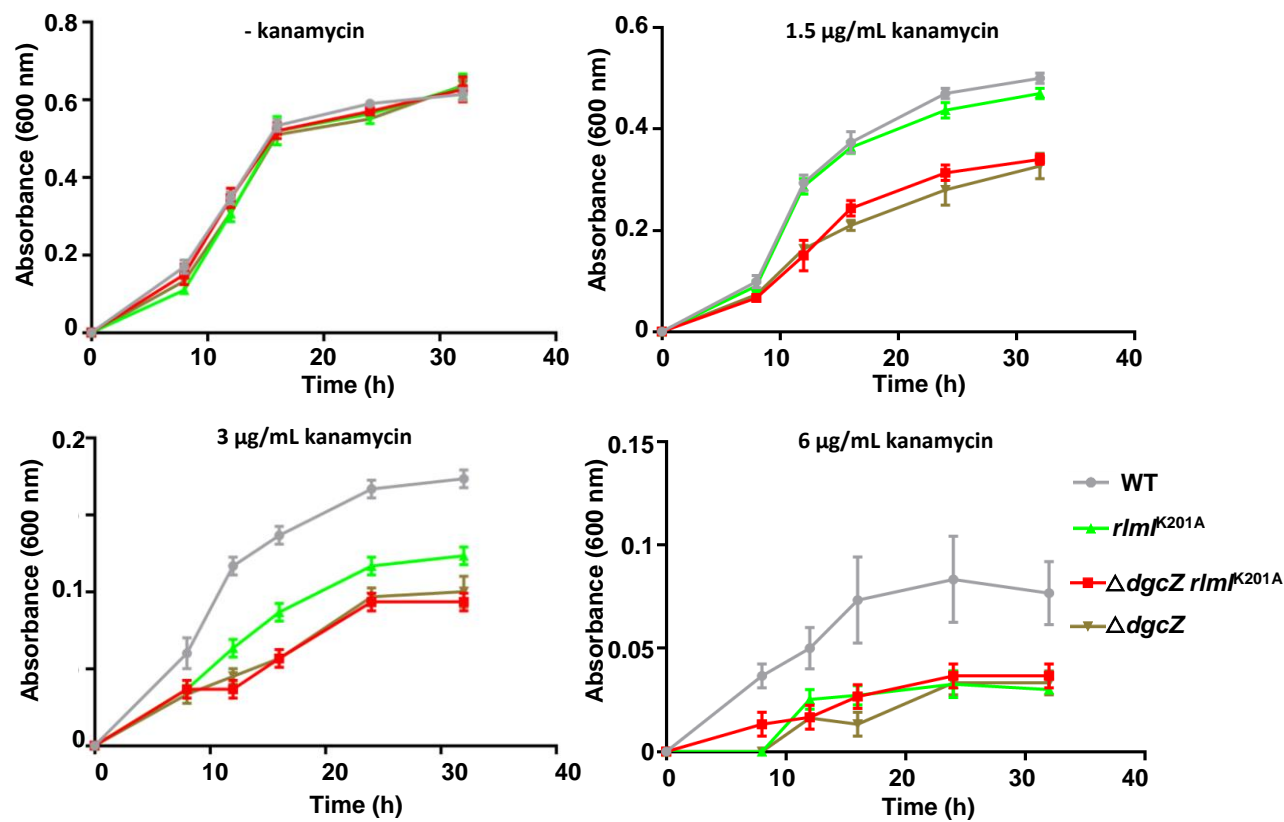
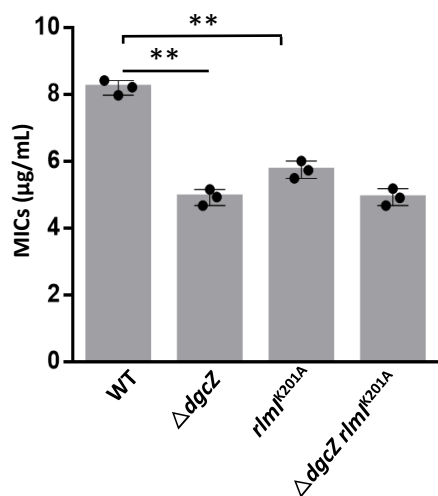
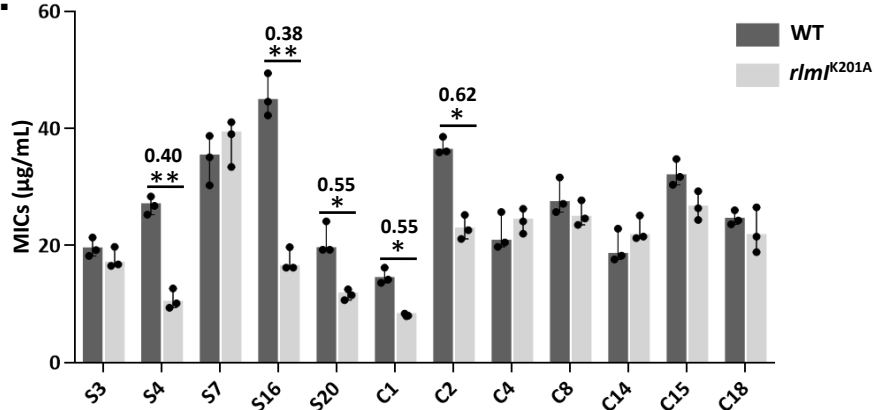
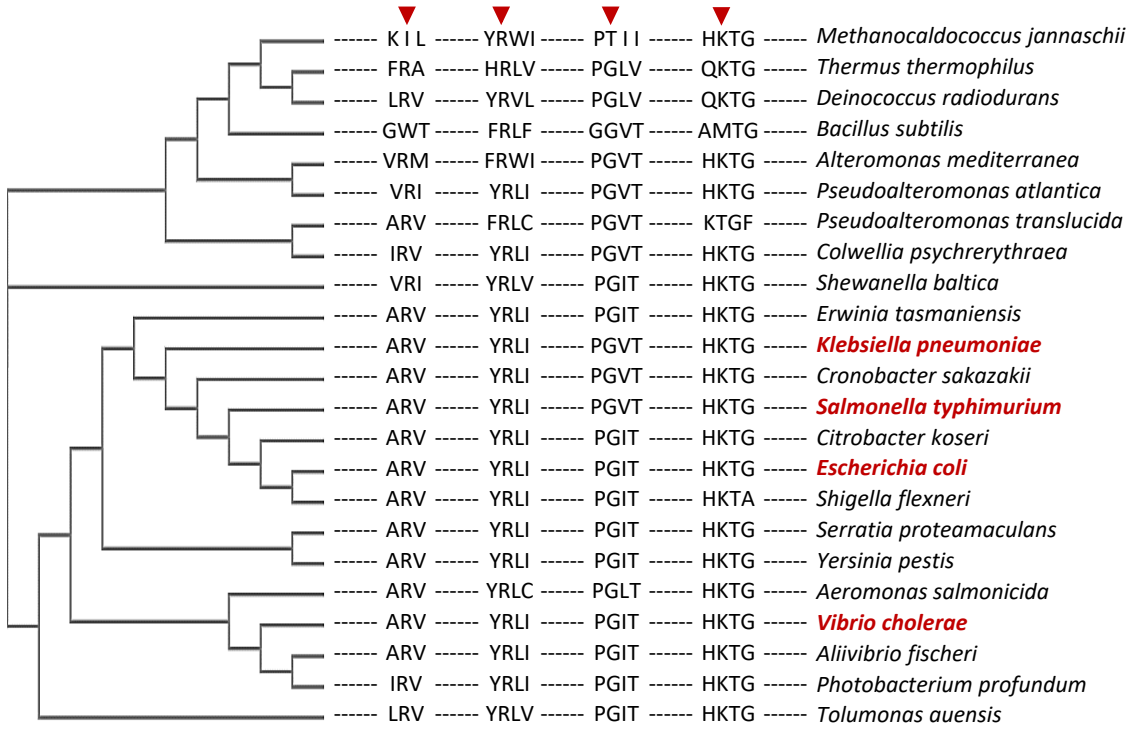
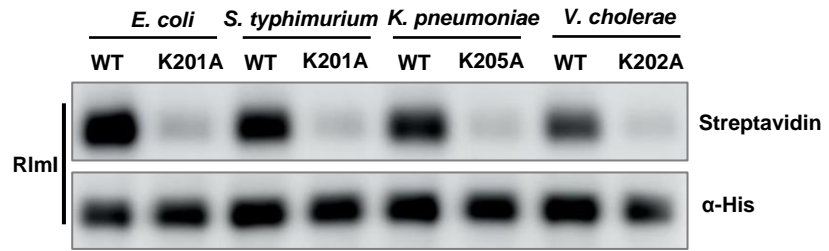
Figure 5**A.****B.****C.****D.****E.**

Figure 6

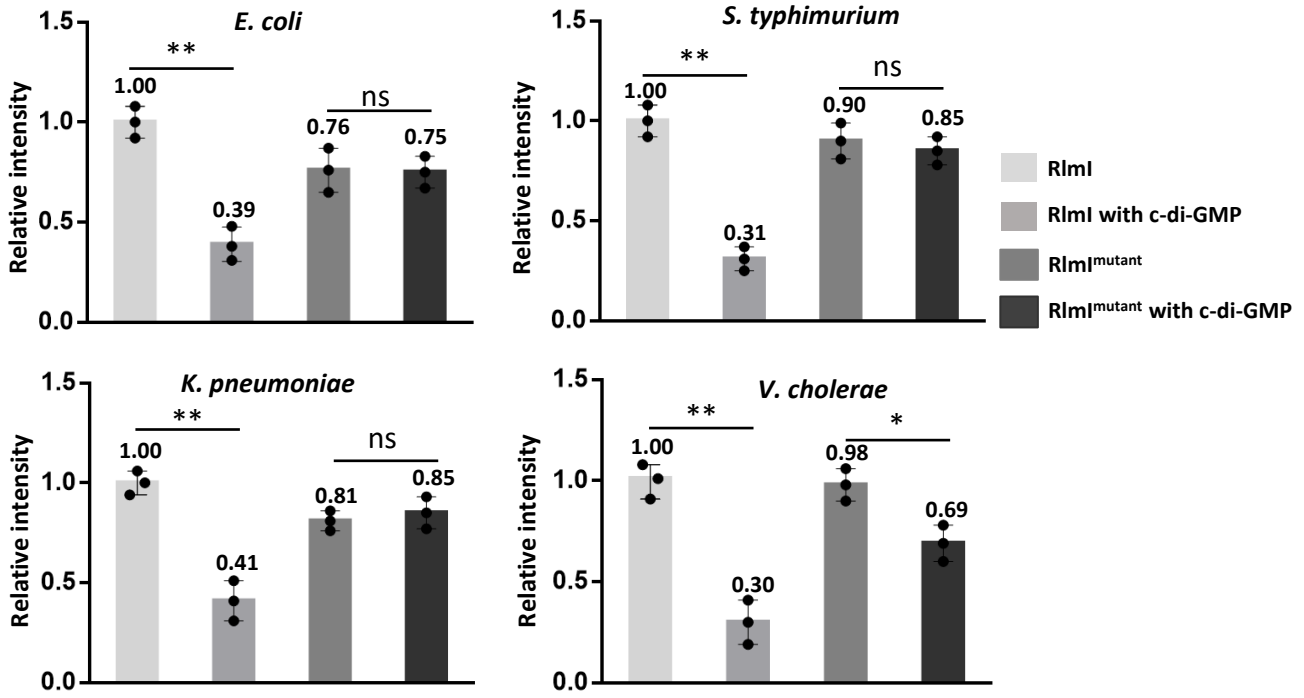
A.



B.

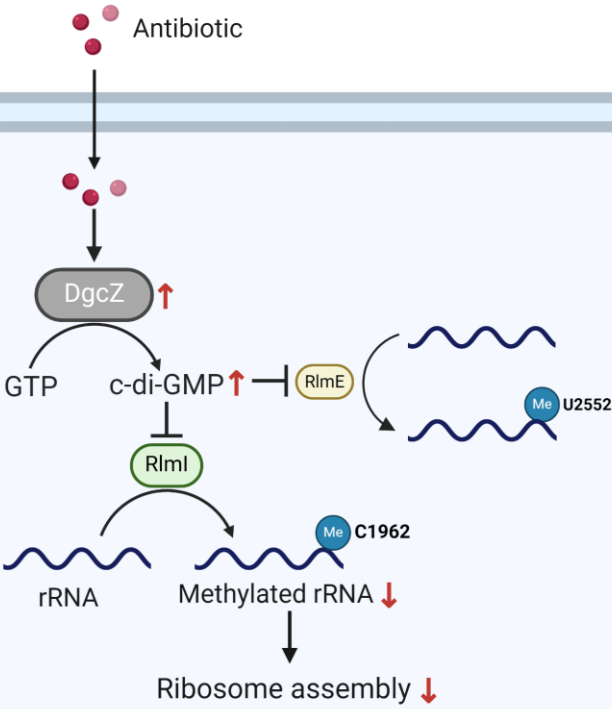


C.



c-di-GMP Inhibits Ribosomal RNA Methylation under Antibiotic Stimulation

Antibiotic stimulation



No antibiotic stimulation

